Bull. Spec. Astrophys. Obs., 1997, 43, 109–132

Results of co-operative observations of SS 433 in the primary minima

S.N. Fabrika[a], V.P. Goranskij[b], V.Yu. Rakhimov[c], A.A. Panferov[a], L.V. Bychkova[a], T.R. Irsmambetova[b], T.K. Manirov[d], S.Yu. Shugarov[b], G.V. Borisov[b]

[a] Special Astrophysical Observatory of the Russian AS, Nizhnij Arkhyz 357147, Russia
[b] Sternberg Astronomical Institute, Moscow, Russia
[c] Institute of Astrophysics, Dushanbe, Tadjikistan
[d] Kazan State University, Kazan, Russia

Received July 11, 1997; accepted July 15, 1997.

Abstract.
Results of spectral and photometric co–operative observations of SS 433 are presented. The spectral observations were carried out with the TV–scanner of the 6 m telescope. The multicolour and V–band photometric observations were made on different telescopes at the Sanglock Observatory of the Tadjik Institute of Astrophysics, the Maidanak Observatory and the Crimean Laboratory of the Sternberg Institute and the Kazan University Laboratory at the Special Astrophysical Observatory. The observations were carried out from 1986 to 1990 at the orbital phase intervals of accretion disk eclipses by the optical star of the binary. The data on seven eclipses obtained at different precession phases of the accretion disk are analysed together. The behaviour of the He II λ 4686 and Hβ emission lines confirms the conclusion made earlier that the line forming regions are eclipsed by the optical star and that the lines are radiated both in the accretion disk region and in the gas stream directed to the disk. It has been found that the absorption P Cyg–type line component of Hβ appears or becomes more intensive in the SS 433 spectrum at the orbital phases near the primary minimum. This transient increasing of the absorptions may be a manifestation of a perturbation in the accretion disk wind behind the optical star.

Key words: stars: close binary: individual (SS 433) — accretion disk — radial velocity

1. Introduction

The close binary system SS 433 is a unique object. There is a supercritical accretion disk and relativistic jets in the system. This binary is an eclipsing one with an orbital period of 13.1 days. Both the disk and jets precess with a precession period of 162.5 days. At the primary minimum (Min I, the orbital phase $\varphi = 0$) the accretion disk is eclipsed by the optical star, the system becomes redder, i. e. the disk is a brighter and hotter component of the binary. The disk precession is displayed in variability of the total brightness and colour indices of SS 433 and in changing eclipse light curve parameters with precession phase ψ. At maximum of the accretion disk opening ($\psi = 0$) the system becomes brighter and bluer and eclipse becomes deeper. In the course of precession H I and He I emission lines formed in the jets move across the spectrum. At $\psi = 0$ their redward and blueward shifts are maximal. A more detailed description of SS 433 photometrical and spectral manifestations can be found in Gladyshev et al. (1987), Kopylov et al. (1987, 1989).

The structure of the supercritical accretion disk as a jet–forming machine is of great interest. Besides SS 433, relativistic jets appear in AGNs and in a few galactic X–ray sources. But SS 433 is the only object where we can directly study this machine because of eclipses and disk precession motion. So it is very important to observe SS 433 during the primary minima at different precession phases, i. e. in different positions of the disk. It has been assumed that it is better to start this program with observations at precession phases $\psi \approx 0$ (the deepest and most regular light curve is in eclipses) as more "simple" phases for interpretation. It is necessary to conduct such observations both in spectral and photometrical modes, which may help to elucidate the structure of the accretion disk and jet bases.

The structure of the accretion disk obtained from these observations is rather complex (Goranskij et al., 1997; Fabrika et al., 1997a, b), it includes of a few components revealed: the "hot spots" — two regions of hot gas (He II cocoons) situated around the

Table 1: *A journal of spectral observations of SS 433*

Eclipse	Date	JD	Phases		λ	n	$\triangle$t
N		2440000+	ψ	φ	(ÅÅ)		
I	01.06.86	6583.50	0.934	0.023	3500 – 5200	1	$0^h\,40^m$
					3700 – 5400	3	1 30
	02.06.86	6584.45	0.940	0.096	3600 – 5300	8	4 00
	03.06.86	6585.43	0.946	0.170	3600 – 5300	7	3 50
	05.06.86	6587.48	0.958	0.327	3600 – 5300	3	4 00
II	03.07.86	6615.48	0.130	0.466	4050 – 5750	2	0 50
	04.07.86	6616.51	0.137	0.546	3800 – 5500	1	0 16
	05.07.86	6617.51	0.143	0.623	3800 – 5500	1	0 20
	08.07.86	6620.51	0.161	0.852	3800 – 5500	1	0 20
	09.07.86	6621.46	0.167	0.925	4000 – 5700	1	0 40
	12.07.86	6624.51	0.186	0.158	4000 – 5700	1	0 20
	14.07.86	6626.52	0.198	0.312	3800 – 5500	1	0 06
	06.06.87	6953.41	0.210	0.301	4300 – 6000	1	1 10
III	28.09.87	7067.17	0.910	0.997	3500 – 5250	1	0 50
	29.09.87	7068.20	0.913	0.076	3500 – 5250	4	2 30
IV	02.09.88	7407.38	0.004	0.004	3600 – 5300	2	1 50
	03.09.88	7408.32	0.009	0.076	3600 – 5300	5	2 00
	05.09.88	7410.38	0.022	0.234	4200 – 5950	1	0 26
V	18.08.89	7757.46	0.158	0.766	3350 – 5050	3	1 20
	19.08.89	7758.46	0.164	0.843	3500 – 5200	2	1 40
	20.08.89	7759.54	0.173	0.925	3600 – 5300	1	0 30
	22.08.89	7761.50	0.183	0.075	3600 – 5300	4	1 50
	24.08.89	7763.48	0.195	0.226	3600 – 5300	2	0 50
VI	06.11.89	7837.42	0.650	0.879	3650 – 5350	3	1 20
	07.11.89	7838.41	0.656	0.954	3800 – 5500	4	2 20
	08.11.89	7839.38	0.662	0.029	3800 – 5500	3	1 20
VII	22.05.90	8034.50	0.863	0.946	3650 – 5350	2	0 50
	23.05.90	8035.48	0.868	0.019	3650 – 5350	3	1 30
	24.05.90	8036.48	0.873	0.095	3650 – 5350	3	1 20
	25.05.90	8037.48	0.881	0.172	3650 – 5350	2	1 20

jet bases, the wind, which is formed in the disk, and the gas stream directed to the disk. The emission line He II λ4686 consists of two components — a broad double–peaked profile, which is totally eclipsed at $\psi = 0$ and formed in the regions around the jet bases and a comparatively narrow intensive component, which is partially eclipsed at $\psi \approx 0.1$ and formed in the stream. Hydrogen and He I emission lines are formed in the stream, or their stream components are dominant in the line profiles. These results have been obtained from co–operative observations of SS 433 in its primary minima. The wind is revealed through in P Cyg–type absorption line components of H I, He I and Fe II, which appear in the SS 433 spectrum in the precession phase interval $0.3 \lesssim \psi \lesssim 0.9$. This phase interval is associated with the disk "edge-on" position, but it is delayed relative to the true "edge-on" by $\triangle\psi \approx 0.1$ (Fabrika et al., 1997 b).

We have performed spectral and photometrical observations of SS 433 during the primary minima at precession phases near $\psi = 0$. The observational data and the results obtained in eclipses I (June 1, 1986) and IV (September 2, 1988) have been published earlier (Goranskij et al., 1987, 1997; Fabrika et al., 1997a). Here we present the observational data for all eclipses (or cycles) observed, including the data published earlier.

2. Spectral observations

The spectral observations have been carried out on the 6 m telescope of the Special Astrophysical Observatory with the 1000-channel TV-scanner (IPCS, Drabek et al., 1986). A spectral dispersion of 1.7 Å/pix provided a resolution of 3 – 4 Å. The blue region has been chosen for spectroscopy as the most informative one, containing the hydrogen lines Hβ, Hγ, Hδ, He I lines λ 5015, λ 4922, λ 4471, He II line λ 4686, the blend C III, N III $\lambda_{\rm eff}$ 4644 and the absorption line Fe II λ 5169. A wavelength range covered by one spectrum is 1700 Å. The method of observations with the TV-scanner, the spectral data reduction and the accuracy of measurements have been described by Kopylov et al. (1985, 1986).

The journal of spectral observations is presented in Table 1. In the table we give the number of the eclipse, the date of observations, JD of the middle of observations during a night, precession and orbital phases, the spectral range covered, the number of spectra taken during a night and Δt – the total time interval of spectral observations during a night. The precession phases were calculated from Margon and Anderson (1989), where $\psi = 0$ corresponds to the T_3 moment of the maximal separation of moving spectral lines formed in the jets or of maximal opening of the disk to the observer:

$$T_3 = \text{JD}\,2443506.78 + 162.50 \cdot \text{E}.$$

The orbital phase $\varphi = 0$ corresponds to Min I or the middle of the accretion disk eclipse by the optical star and is calculated as (Fabrika et al., 1990):

$$\text{Min I} = \text{JD}\,2445942.217 + 13.0813 \cdot \text{E}.$$

All the observations are presented according to their eclipse number. There are seven cycles under study in Table 1 (from I to VII, covered by 29 nights of observations), which are different in precession phases or in accretion disk orientations. The precession phases of cycles I and III ($\psi = 0.91 \div 0.96$), II and V ($\psi = 0.13 \div 0.20$) are about the same inside the pairs, so, these eclipses can be analysed together. The observation on June 6, 1987 is very close in its precession phase to eclipse II, so, this can be also studied together with the data of cycle II.

In Figs. 1–5 we present the spectra obtained in counts. The sky substracted spectra were shifted along the vertical axis or multiplied by a constant value (see the figure captions for details) for the best presentation of the data. Identification of the main stationary lines is presented in the figures: 1 – Hϵ, 2 – Hδ, 3 – Hγ, 4 – He I λ 4471, 5 – C III, N III $\lambda_{\rm eff}$ 4644, 6 – He II λ 4686, 7 – Hβ, 8 – He I λ 4922, 9 – He I λ 5015. The strongest moving lines in the region are Hβ^- and Hγ^+, which are applied numbers 4 and 10 on the spectra of cycles I and III (Fig. 1). There are also moving lines observed during these eclipses, Hγ^- (near the position of Hϵ), Hϵ^+ (at $\lambda \approx 4550 \div 4600$) and H$\delta^+$ (between He II λ 4686 and Hβ), but these lines are not so strong as to distort notably the stationary lines. During cycles II and V (Fig. 2) the separation of the moving lines is a little smaller, than in the previous cycles, but their intensity is not so high. The lines Hβ^- and Hγ^+ are clearly seen at $\lambda \approx 4650$ and, correspondingly, in the blue wing of Hβ on the dates JD 2446953 and 7763 during these eclipses and probably on JD 2446624 and 6626. On the dates JD 2446617 – 6621 of eclipse II and on JD 2447757 – 7761 of eclipse V the Hγ^+ and Hβ^- lines move to one another. On other dates (JD 2446615, 6617) the separation between the moving lines is greater. Identification of the moving lines in the blue spectrum of SS 433 is not easy since the lines are too crowded there, and because of a time delay between variations of the red and blue jet lines, the lines sporadic variability and because of the 6-days' nutation motion. The latter shifts the lines up to 100 Å. Nevertheless a few moving lines still remain unidentified in this region (Goranskij et al., 1987).

At the precession phases of eclipse IV (Fig. 3) the moving lines separation is maximum and similar to that of cycle I. During eclipse VI (Fig. 4) the separation is minimum over all the observations presented in the paper. The strongest moving lines are Hβ^+ (labeled by 10 in the figure) and Hβ^- (labeled 4). The latter moves from Hβ to He I λ 4922 during the observations. The two Hγ relativistic lines are situated at the stationary line Hγ and at $\approx \lambda$4550. In the spectra on the dates JD 2447838 – 7839 one can see the He I$^+\lambda$ 4922 and He I$^+\lambda$ 5015 lines in the region $\lambda\lambda$ 5300 – 5400. During cycle VII the Hβ^- line (Fig. 5, number 4) moves in the course of nutation motion redward until JD 2448036 and blueward on 8037. The Hδ^+ (between λ4720 and λ4780) and Hγ^+ lines (near He I λ 5015) move reverse.

In Table 2 we present the results of measurements of the line parameters: equivalent width W_λ, line intensity expressed in units of continuum intensity R_c, FWHM, radial velocities of the line centre of mass V_c and the line peak V_p for the stationary lines Hγ, Hβ, He II λ 4686, He I λ 4922 and He I λ 5015. A description of the measurement accuracy and line parameter determination one can find in Kopylov et al. (1985, 1986). In doubtful cases of very structural line profiles, of lines blended by moving relativistic lines the results are not listed in the table or they are marked by a colon.

3. Photometrical observations

The results of multicolour photometrical observations are presented in Table 3 and V-band observations in

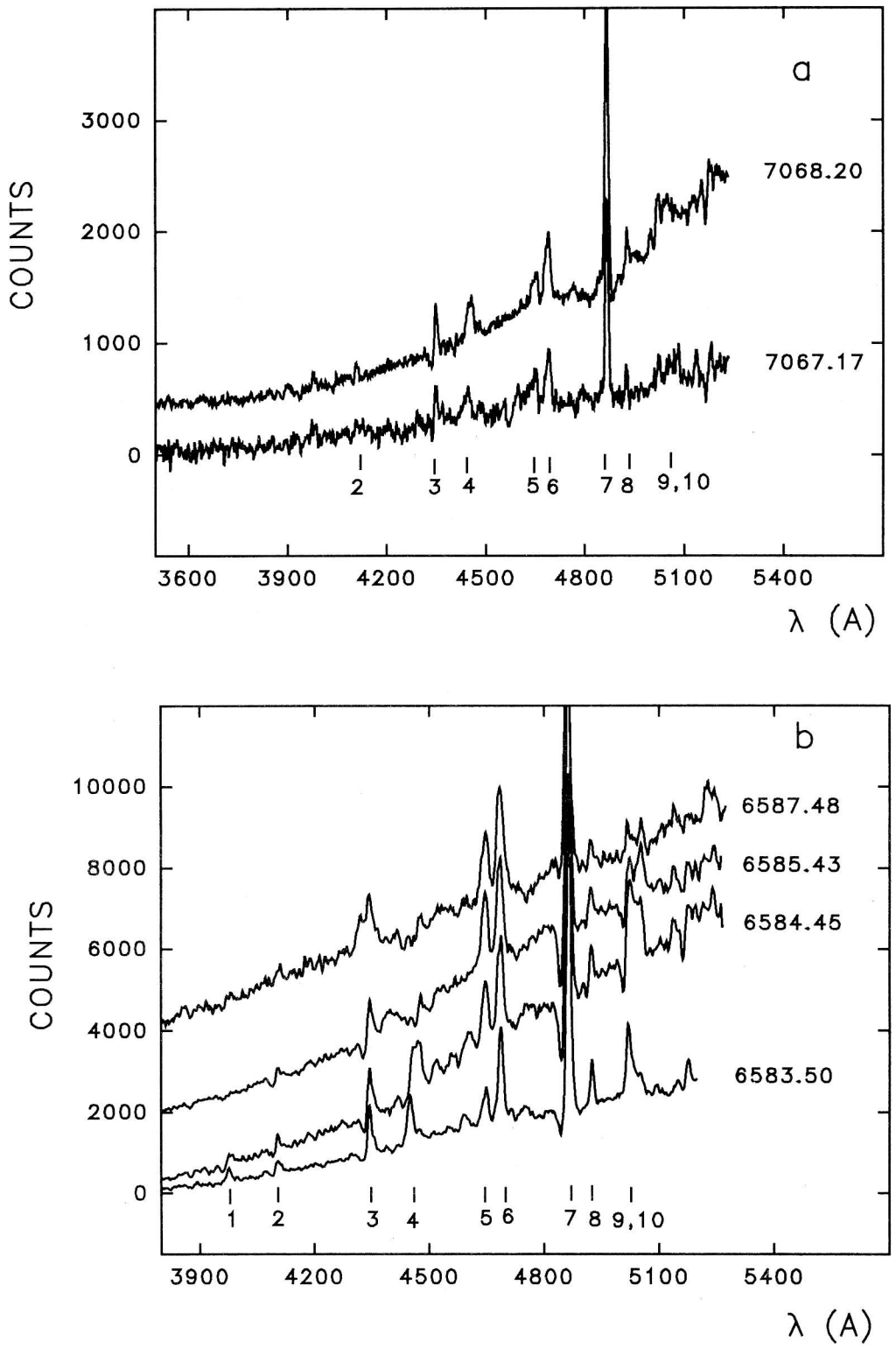

Figure 1: *Spectra of SS 433 obtained in cycles III (a) and I (b). The spectra are marked by a date (JD 2440000 +). Identification of the main lines is also shown: 1 – Hε, 2 – Hδ, 3 – Hγ, 4 – He I λ 4471 (and Hβ⁻), 5 – C III, N III* $\lambda_{\rm eff}$ *4644, 6 – He II λ 4686, 7 – Hβ, 8 – He I λ 4922, 9 – He I λ 5015, 10 – Hγ⁺. The spectra were shifted along the vertical axis or multiplied by a constant value: 6583.50 –* ×1.2, *6584.45 –* ×1.2+200, *6585.43* +1900, *6587.48 –* ×4.0 + 3900, *7067.17 –* ×3.0, *7068.20 –* +200.

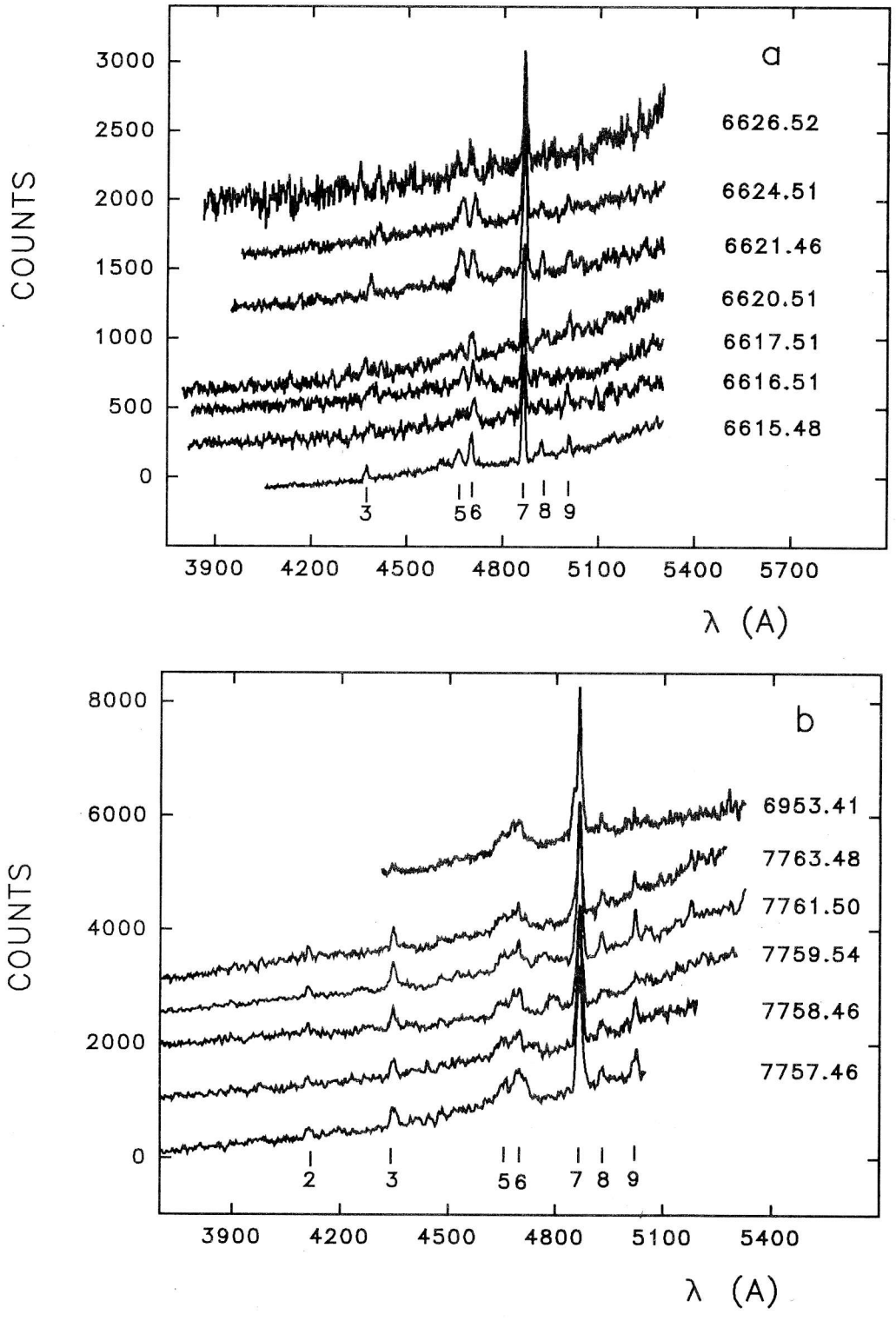

Figure 2: *Spectra of SS 433 obtained in cycles II (a) and V (b). Other notations are the same as in Fig. 1. The spectra were shifted along the vertical axis or multiplied by a constant value: 6615.48* – $\times 0.25 - 100$, *6616.51* – $\times 1.2 + 200$, *6617.51* – $\times 1.2 + 400$, *6620.51* – $+600$, *6621.46* – $+1200$, *6624.51* – $+1600$, *6626.52* – $\times 3.5 + 2000$, *7758.46* – $\times 1.6 + 1000$, *7759.54* – $\times 1.3 + 1900$, *7761.50* – $\times 0.7 + 2500$, *7763.48* – $\times 1.5 + 3000$, *6953.41* – $\times 2.0 + 4800$.

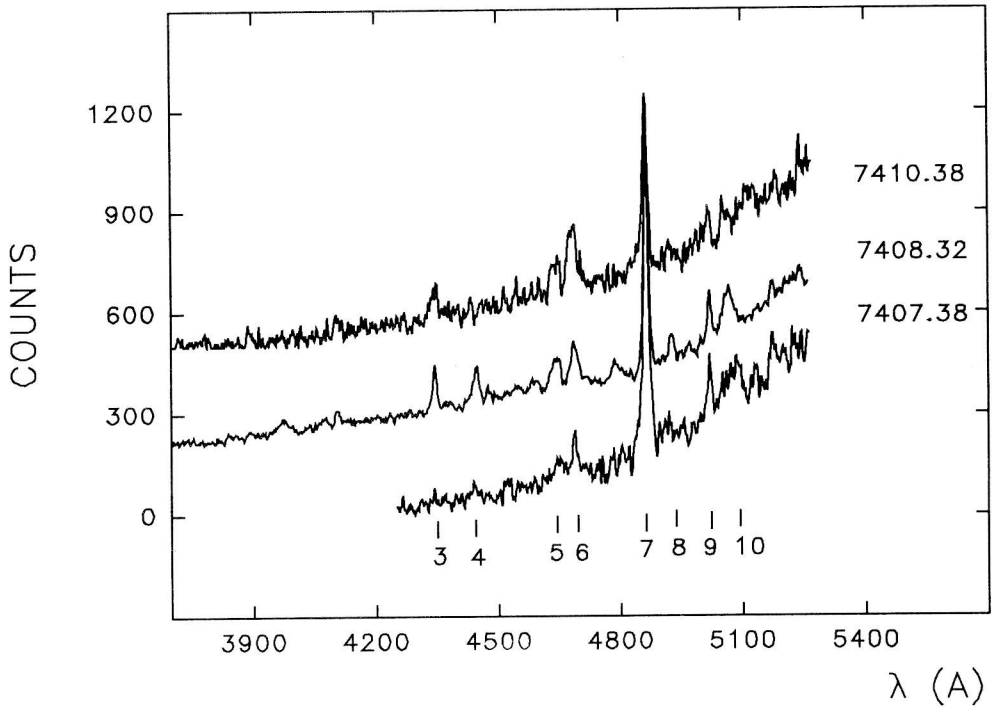

Figure 3: *Spectra of SS 433 obtained in cycle IV. Other notations are the same as in Fig. 1. The spectra were shifted along the vertical axis or multiplied by a constant value: 7408.32 – +200, 7410.38 – ×1.5 + 500.*

Table 4. The first column in the tables is the number of the cycle, the last one gives the observer. We present below the data of cycle II, the observations obtained on JD 2446939 – 6951, which are very close in their precession phase to eclipse II. Every photometrical observation consists of different numbers (from 1 to 60) of individual measurements. The JD is the moment of the middle of observation. Photometrical data obtained in cycles I and IV have already been described by Goranskij et al. (1987, 1997). Some of the data have also been published in Gladyshev et al. (1987), Goranskij et al. (1987), Gladyshev and Irsmambetova (1989), Irsmambetova (1997).

The multicolour U B V R I observations were carried out on the 1 m telescope (Kayumov et al., 1989) at the Sanglock Observatory of the Tadjik Institute of Astrophysics (see also Goranskij et al., 1987; 1997). The accuracy of individual measurements is $\sigma(U) = 0^m.1$, $\sigma(B) = 0^m.06$, $\sigma(V) = 0^m.03$, $\sigma(R) = 0^m.01$, $\sigma(I) = 0^m.03$. The multicolour B V R observations (marked "ir" in the tables) were carried out on the 1 m and 0.6 m telescopes at the Maidanak Observatory of the Sternberg Institute. The average accuracy of individual measurements of these observations (see for details Irsmambetova, 1997) is $\sigma(B) = 0^m.03 - 0^m.08, \sigma(V) = 0^m.01 - 0^m.03, \sigma(R) = 0^m.006 - 0^m.02$. Photometrical B V observations were also carried out on the 0.6 m and 1.25 m telescopes of the Crimean Laboratory of the Sternberg Institute (see Goranskij et al., 1997; Gladyshev et al., 1987). These data are marked in Table 3 by "gr" or "sh" and "pe" in Table 4. Another observing site was the Kazan University Laboratory at the Special Astrophysical Observatory. The B V observations were carried out on the 0.6 m telescope with the photometer "EPHIR" (see Neizvestny, Pimonov, 1978; Neizvestny et al., 1980). The average accuracy of these individual measurements marked by "m" in the tables is $0^m.05 \div 0^m.07$. The V–band photographic observations were carried out on the 0.5 m telescope of the Crimean Laboratory of the Sternberg Institute (Goranskij et al., 1997). The latter are marked by "ph" in Table 4. All these photometric data have been reduced using the standard star C_1 and its fluxes ($V = 11^m.42$) published by Goranskij et al. (1987, 1997).

In cycle VII on May 20, 1990 we made a high-speed photometry of SS 433 on the 1.25 m telescope of the Crimean Laboratory of the Sternberg Institute. The device used was a three–beam, pulse–counting photometer (Borisov, 1992). The continuous V–band observation (the object, the comparison star and the sky background) was carried out during 2.2 hours with an integration time of 2 s and a resolution time of 6.5 s. As the comparison star a blue star (BS) was used, which is situated about 8′ exactly to the East of SS 433. A rough estimate of the BS brightness made later is $V \approx 13^m.5$.

The results of the photometrical observations are also presented in Figs. 6 – 11. Figs. 6 – 9 give individual light curves and colour curves in the eclipses.

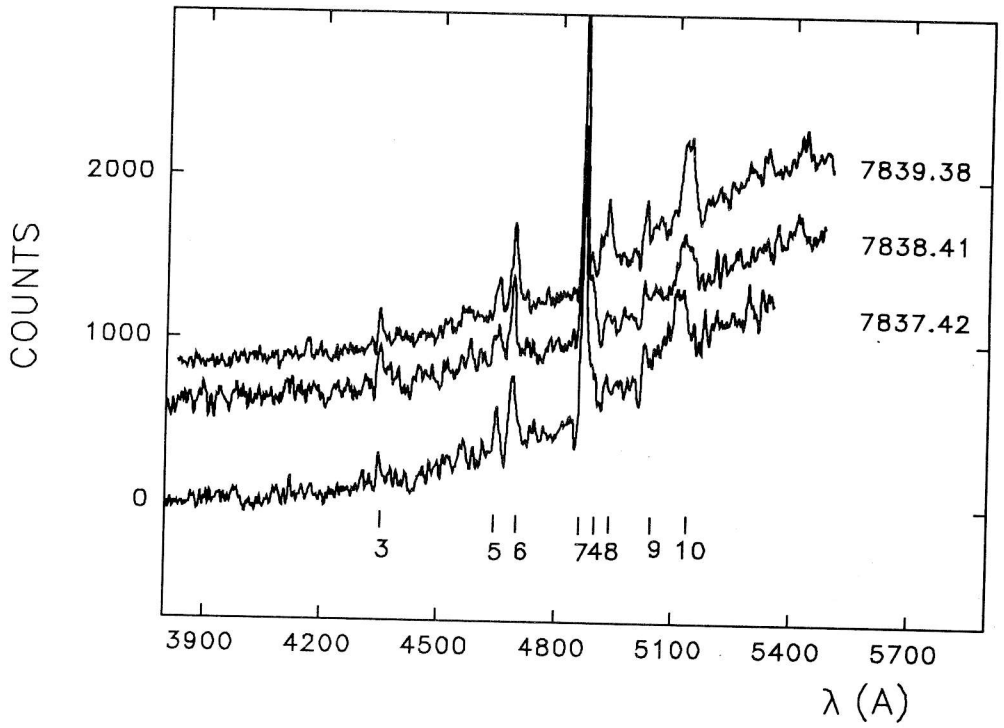

Figure 4: *Spectra of SS 433 obtained in cycle VI. Other notations are the same as in Fig. 1. The spectra were shifted along the vertical axis or multiplied by a constant value: 7838.41 – +600, 7839.38 – +800.*

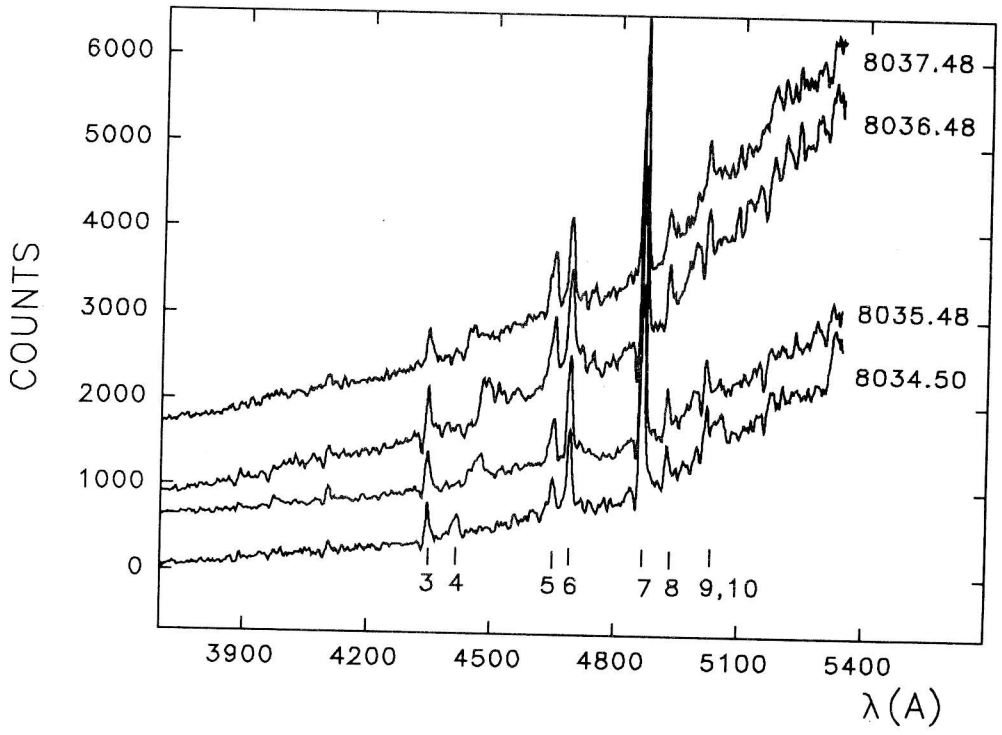

Figure 5: *Spectra of SS 433 obtained in cycle VII. Other notations are the same as in Fig. 1. The spectra were shifted along the vertical axis or multiplied by a constant value: 8034.50 – ×1.3, 8035.48 – +600 8036.48 – +800, 8037.48 – +1200.*

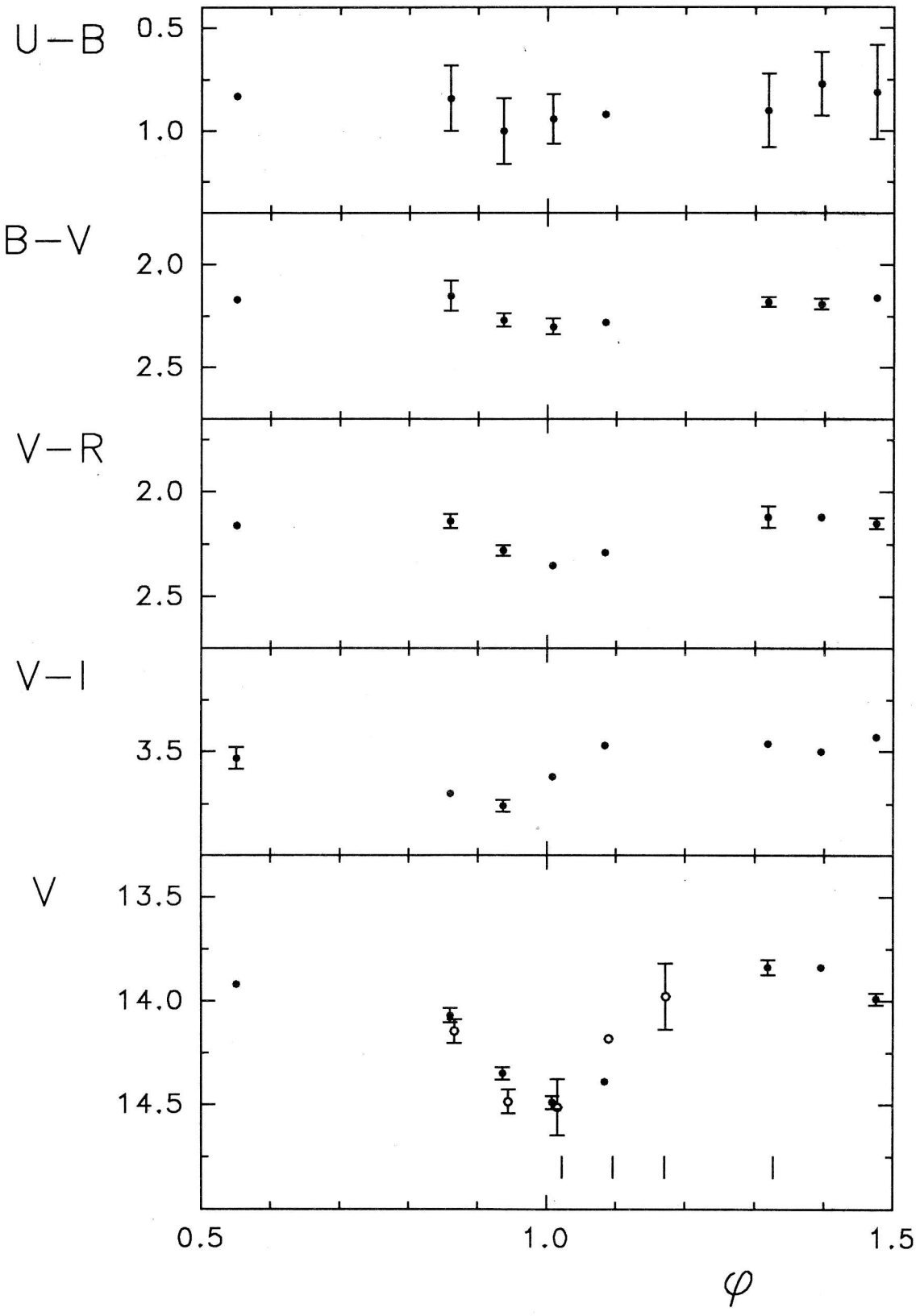

Figure 6: *Photometrical behaviour of SS 433 during cycle I. Every point corresponds to one night and one telescope. Vertical bars mark the moments of spectral observations. Filled circles — observations in Sanglok, open circles — observations in Crimea (see also Goranskij et al., 1987).*

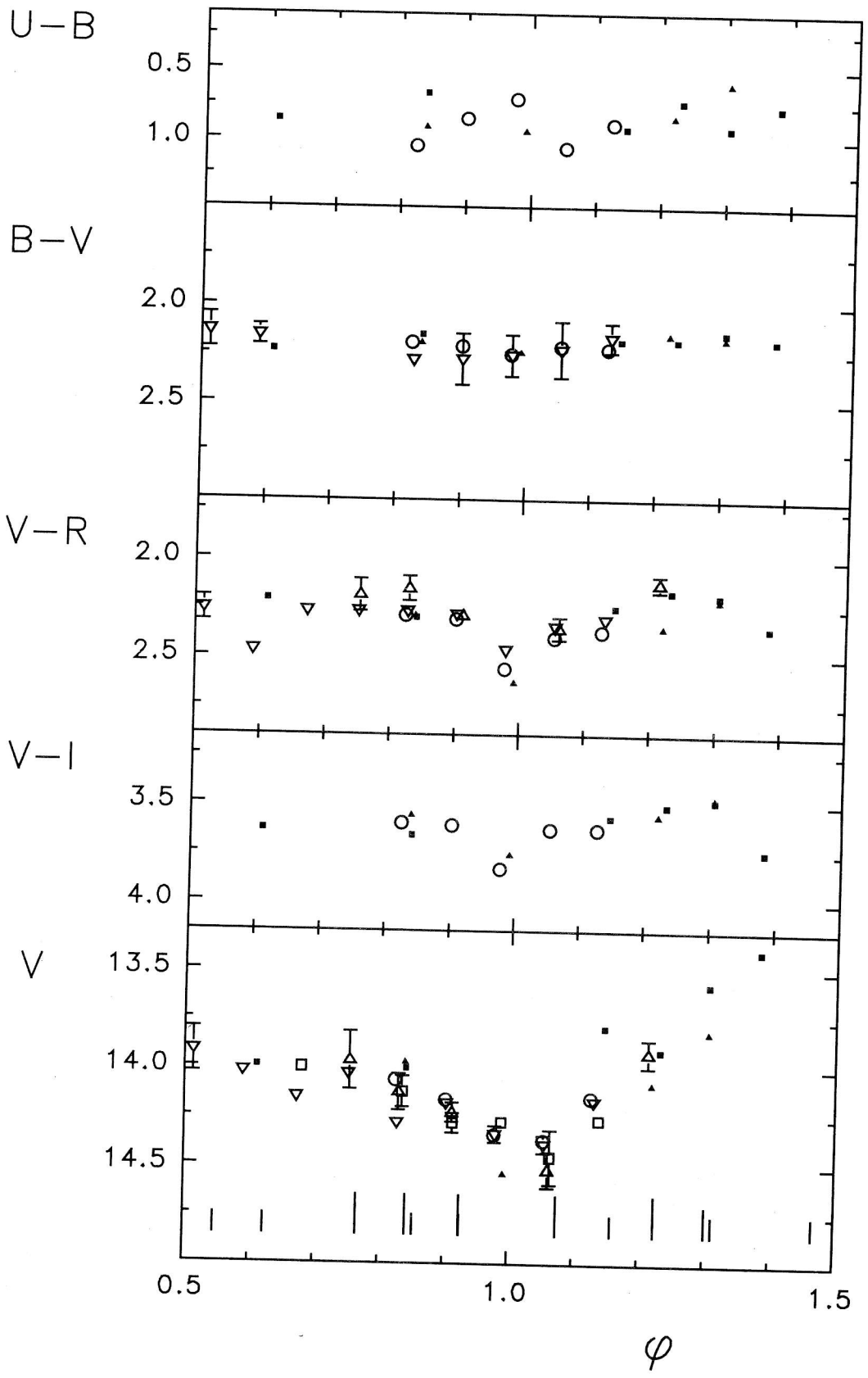

Figure 7: *Photometrical behaviour of SS 433 during the cycles II and V. Observations in Sanglok are marked by filled triangles (cycle II), filled squares (JD 2446939 - 6951) and open circles (cycle V); Crimea — open squares, SAO — open triangles, Maidanak — open turn over triangles (cycle V). Vertical bars mark the moments of spectral observations. different cycles differ in the bars' length (see Tabl. 1).*

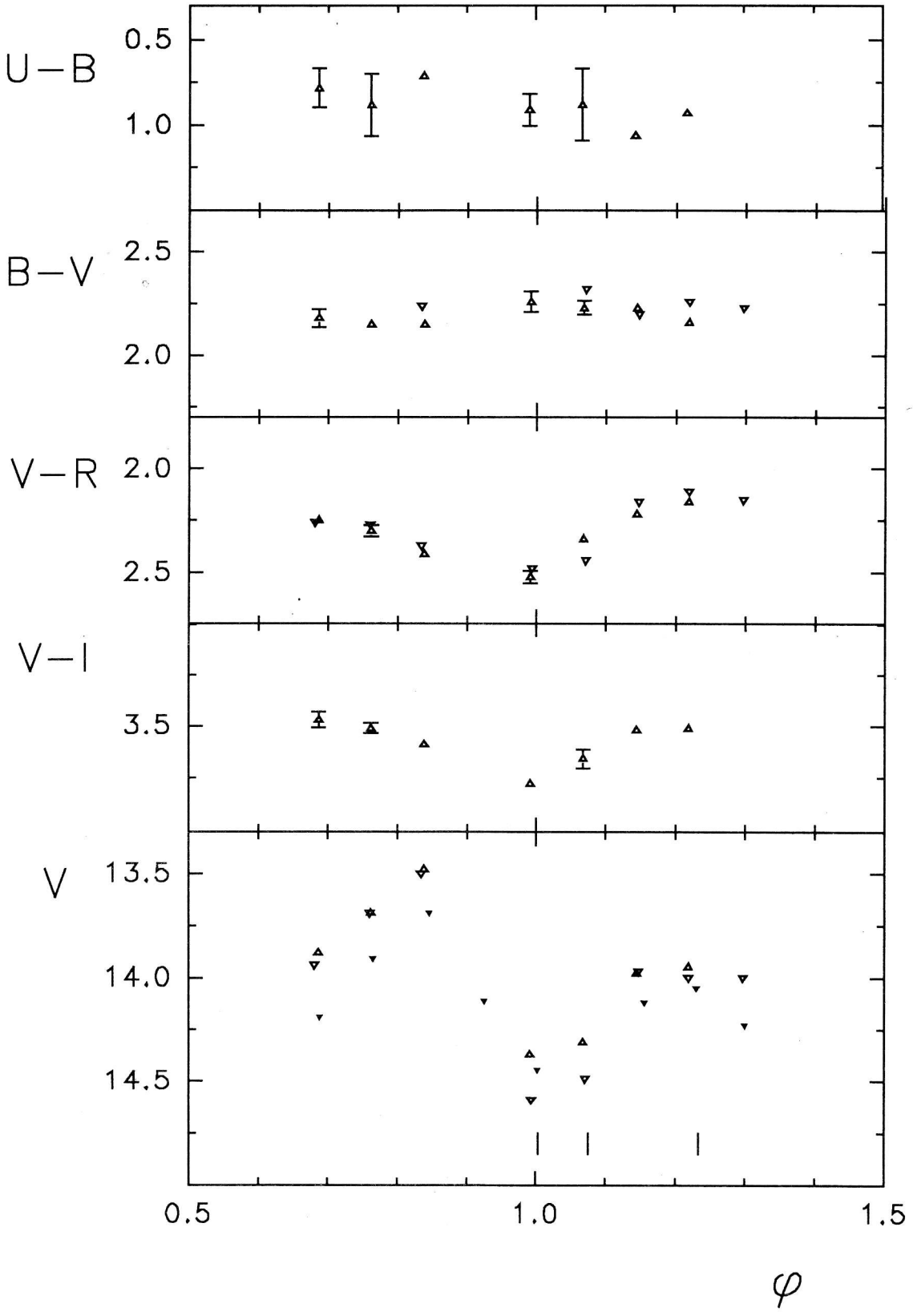

Figure 8: *Photometrical behaviour of SS 433 during cycle IV. Observations in Sanglok are marked by open triangles, Crimea — filled turn over triangels, Maidanak — open turn over triangles.*

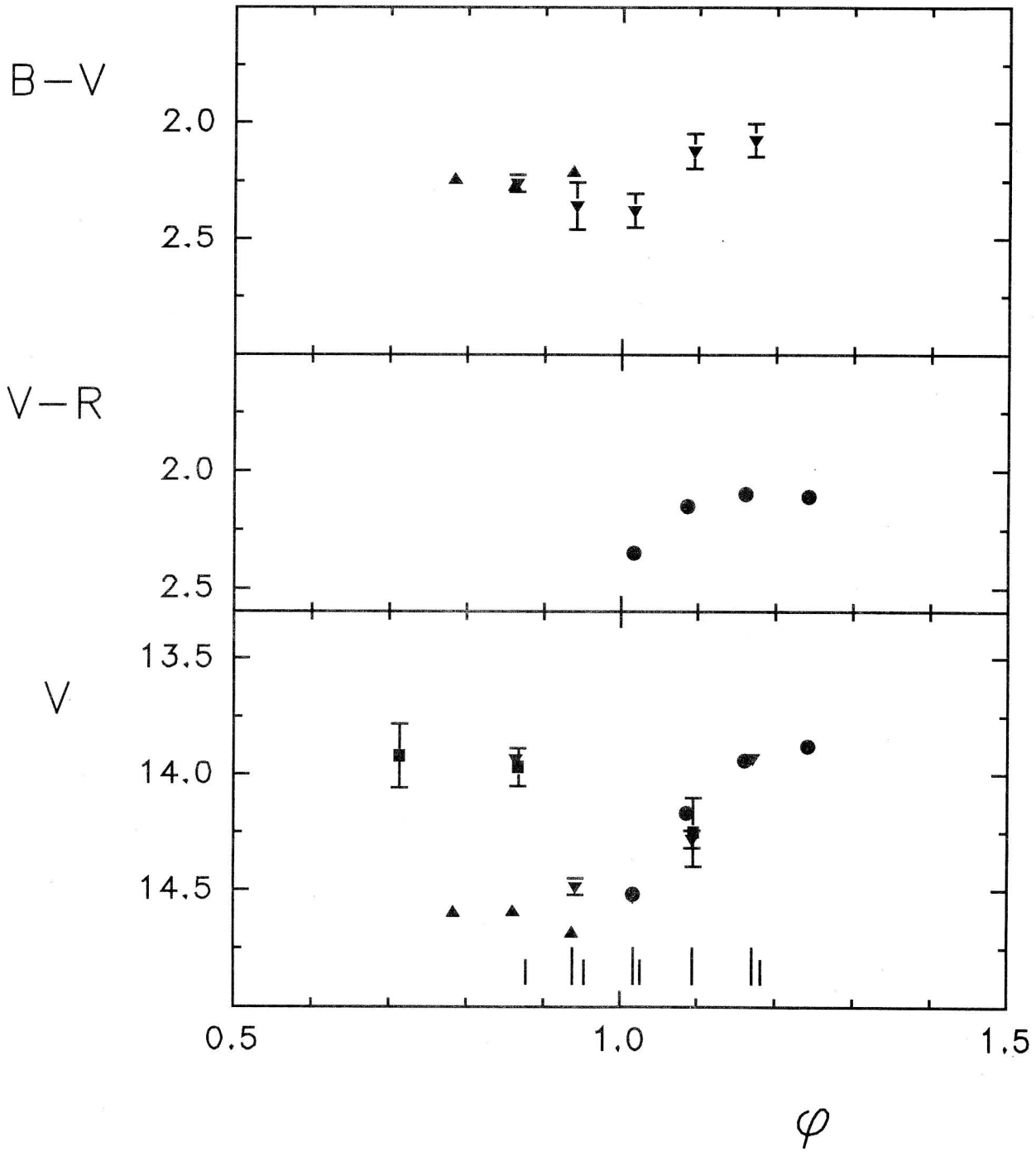

Figure 9: *Photometrical behaviour of SS 433 during cycles VI and VII. Cycle VI — filled triangles (Crimea), cycle VII — filled turn over triangles (Crimea), filled squares (SAO) and filled circles (Maidanak).*

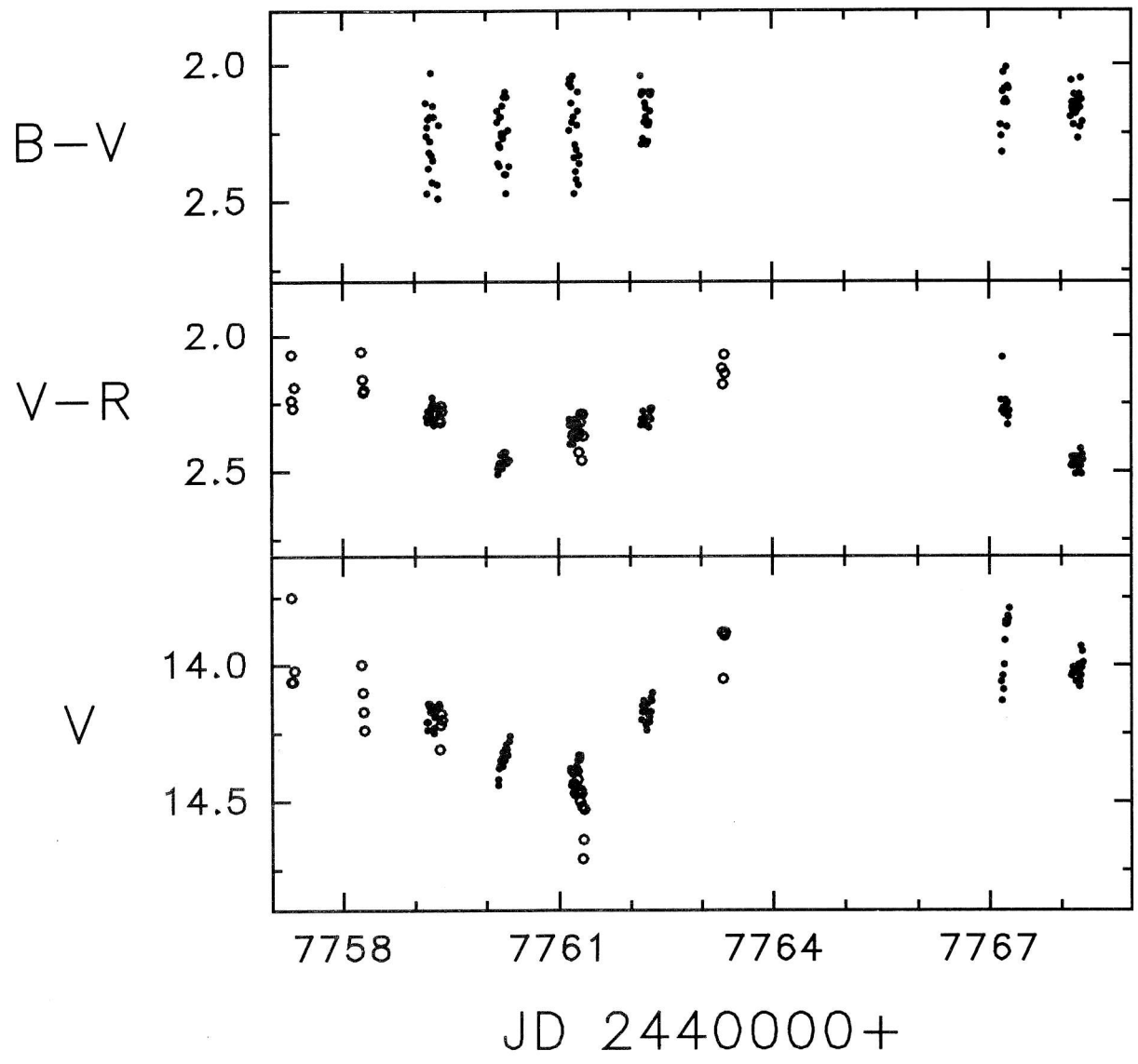

Figure 10: *Individual photometrical observations obtained during the eclipse V at Maidanak (filled circles) and at SAO (open circles).*

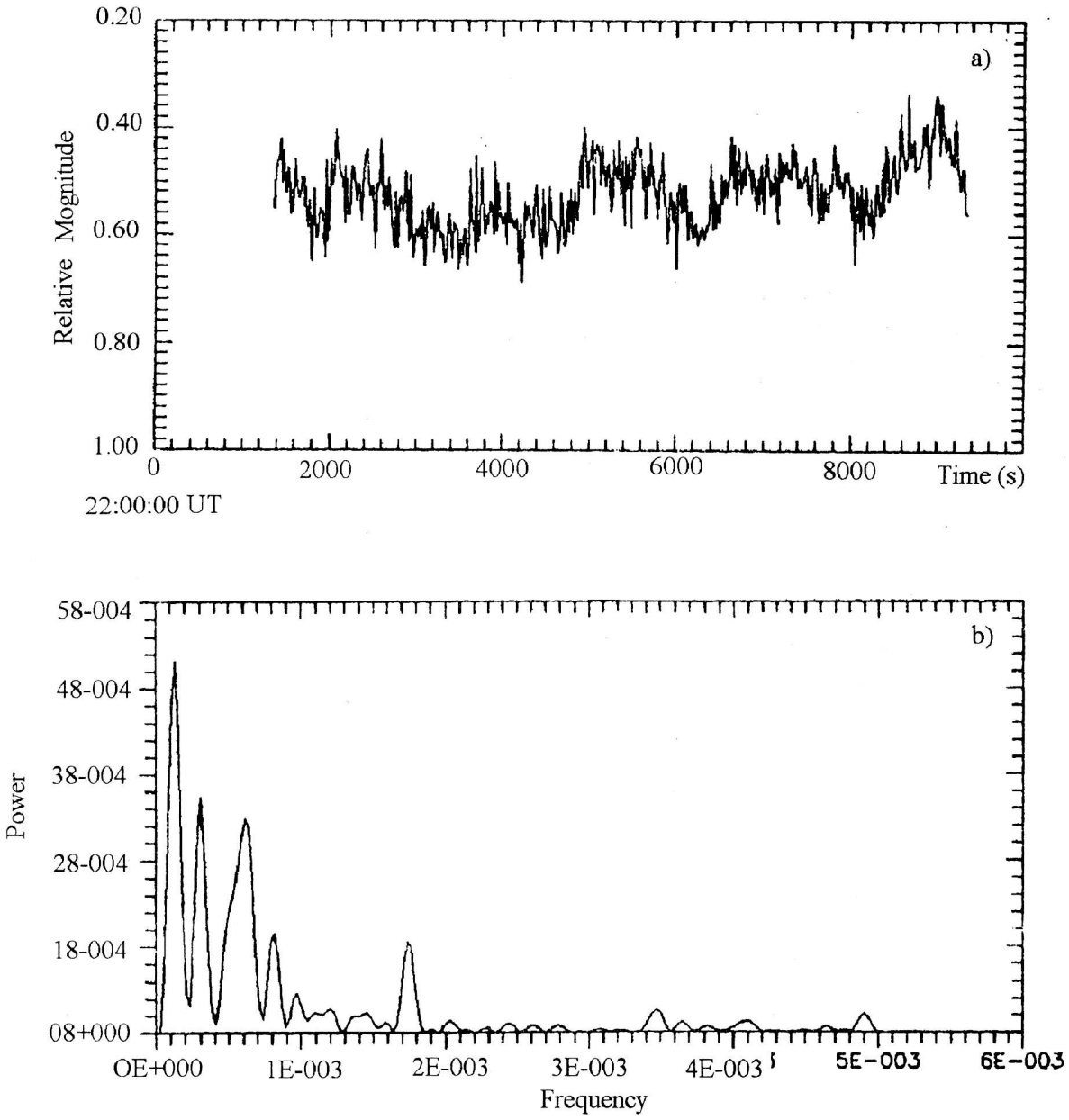

Figure 11: *a — V-band light curve obtained with the three-beam, pulse-counting photometer on May 20, 1990 (eclipse VII). b — the Fourier power spectrum (frequency in units* 10^{-3} *Hz).*

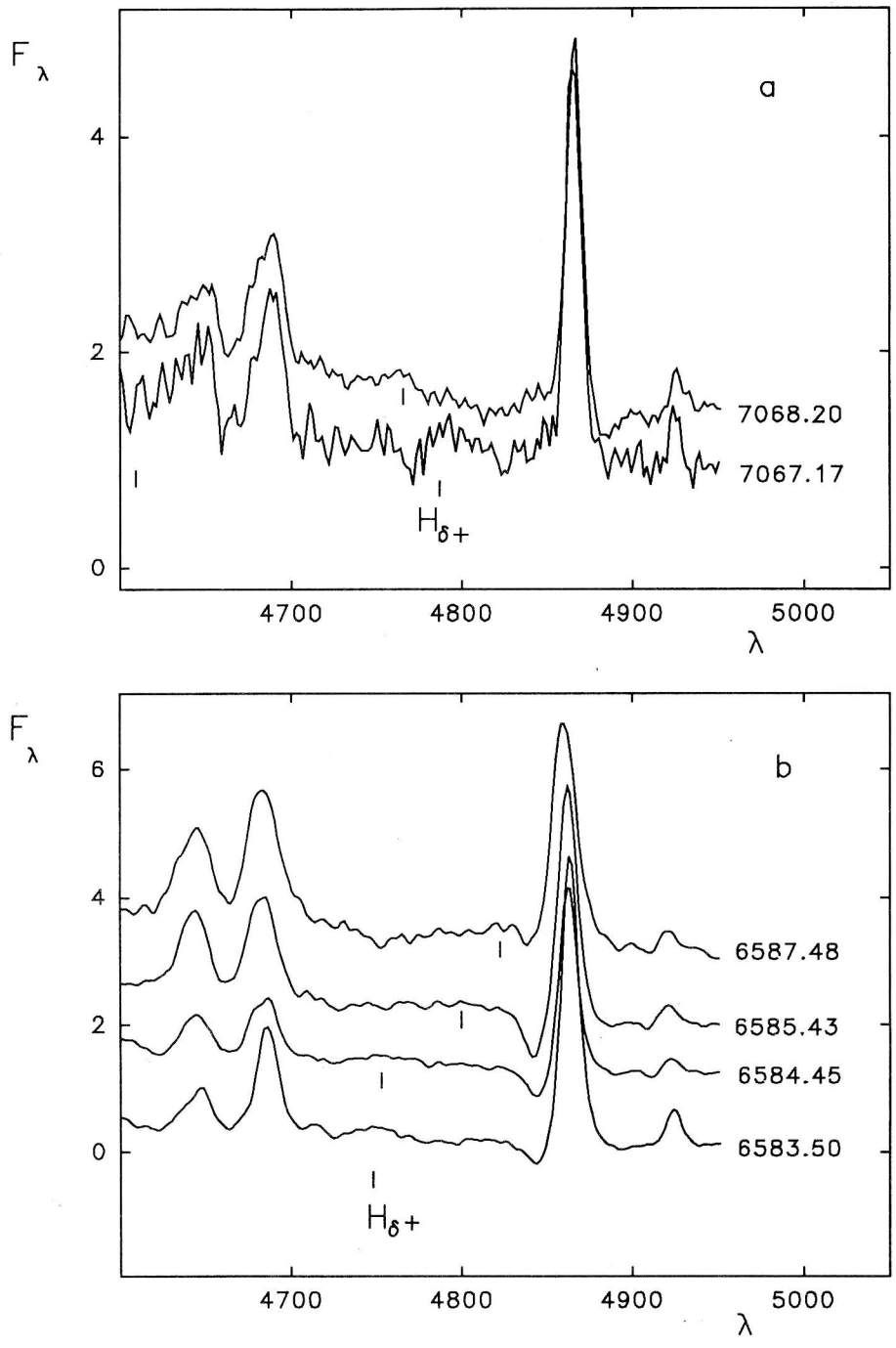

Figure 12: *Fragments of the spectra obtained in cycles III (a) and I (b). The spectra corrected for interstellar absorption are in units* 10^{-11} erg/cm^2 s Å. *Position of the moving lines* $H\delta^+$ *and* He^+ *are marked by vertical bars. Some of the spectra were shifted along the vertical axis: 6583.50 – −1, 6587.48 – +1.*

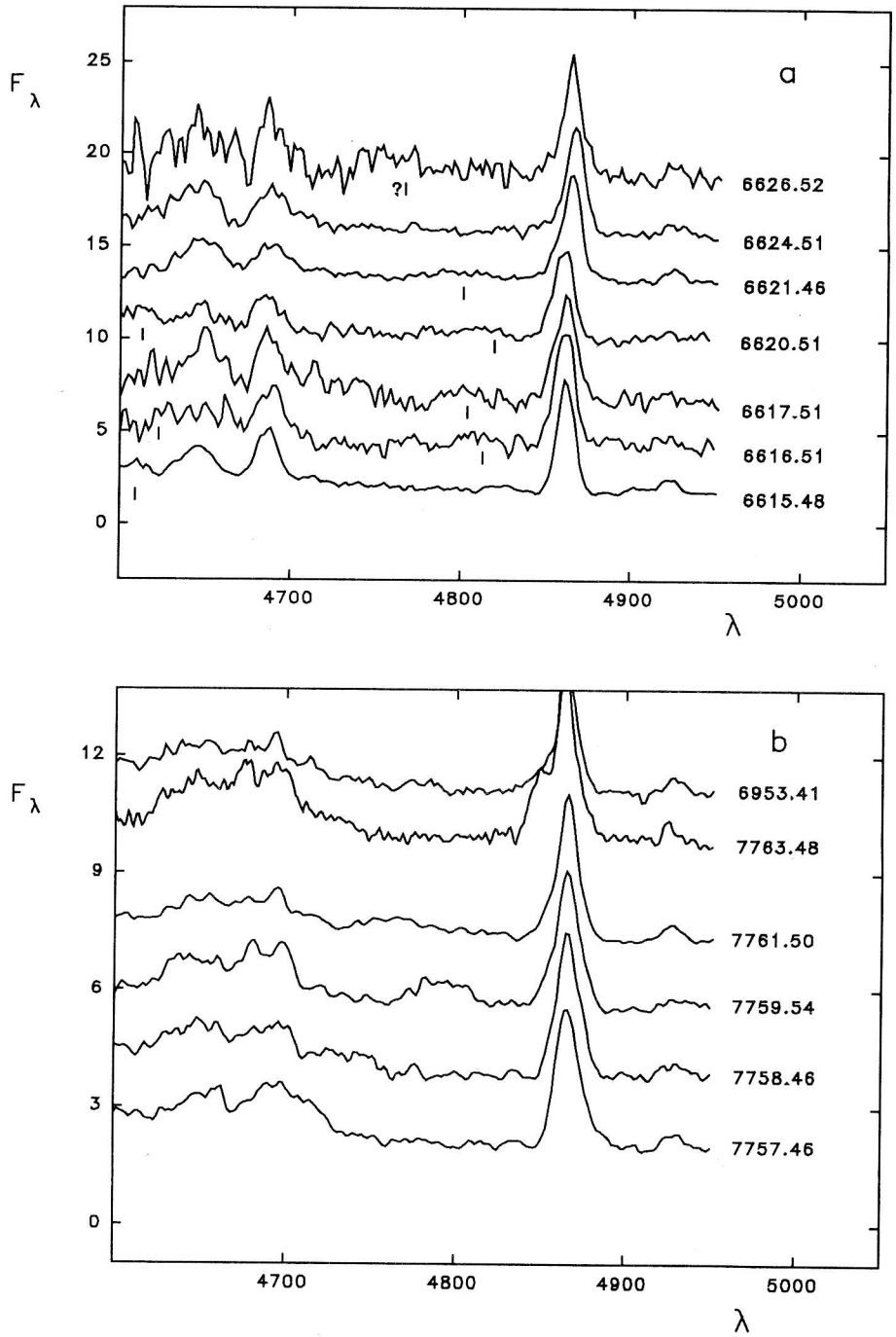

Figure 13: *Fragments of the spectra obtained in cycles II (a) and V (b). Position of the moving lines $H\gamma^+$ (right) and $H\beta^-$ (left) were marked by vertical bars. In complicated cases the positions were not marked. The spectra were shifted along the vertical axis: 6616.51 – +2, 6617.51 – +4, 6620.51 – +8, 6621.46 – +12, 6624.51 – +14, 6626.52 – +17, 7758.46 – +2, 7759.54 – +4, 7761.50 – +6, 7763.48 – +8, 6953.41 – +9. The units are the same as in Fig. 12.*

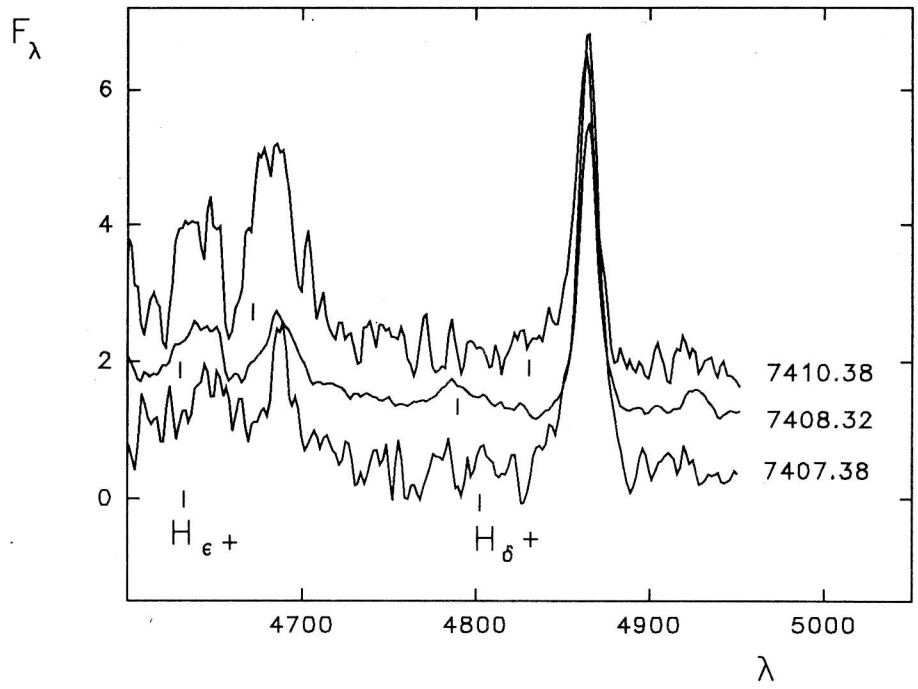

Figure 14: *Fragments of the spectra of SS 433 obtained in cycle IV. The spectrum for JD 2447407.38 was shifted along the vertical axis on −1. The units are the same as in Fig. 12.*

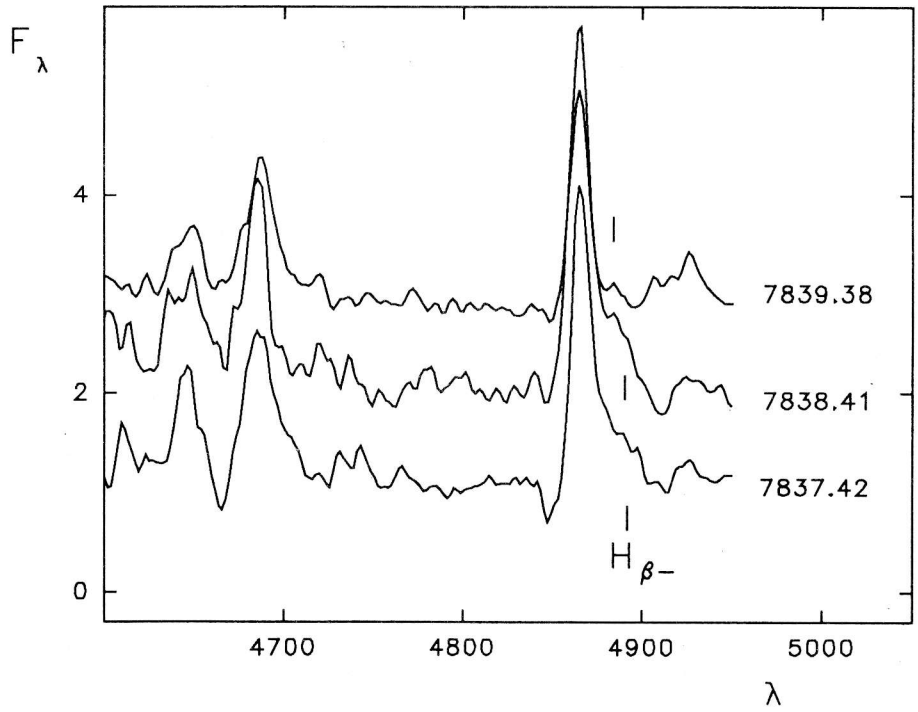

Figure 15: *Fragments of the spectra of SS 433 obtained in cycle VI. The spectra were shifted: 7838.41 − +1, 7839.38 − +2. The units are the same as in Fig. 12.*

Table 2: *Parameters of emission lines*

JD 2440000+	W_λ (Å)	R_c	FWHM (Å)	V_c (km/s)	V_p (km/s)	W_λ (Å)	R_c	FWHM (Å)	V_c (km/s)	V_p (km/s)
	Hβ					Hγ				
6583.50	52	4.1	11	180	120	19	1.3	11	400	210
6584.45	29	2.3	12	130	80	10	0.7	13	380	160
6585.43	24	1.8	13	90	60	8	0.5	14	440	200
6587.48	30	1.6	16	10	−130					
6615.40	43	3.4	12	−10	−40	21	1.6	11	150	240
6616.51	56	3.6	15	10	10					
6617.51	57	3.1	17	−60	−10					
6620.51	51	3.2	14	10	70					
6621.46	77	4.8	13	170	230	23	1.7	14	270	310
6624.51						27	1.9	14	150	50
7067.17	39	3.0	13	340	310	15	1.1	13	580	590
7068.20	27	1.9	13	190	300	13	1.0	12	600	370
7407.38	95	5.4	14	100	190	24	2.5	5	110	200
7408.32	44	3.2	12	200	200	18	1.3	12	280	300
7410.38						23	1.3	25	80	590
7757.46	33	1.8	17	390	210	13	0.6	20	580	210
7758.46	36	2.2	16	320	260	14	0.8	18	470	650
7759.54	40	2.2	15	280	280	20	1.1	13	620	530
7761.50	44	2.8	13	230	280	20	1.0	16	460	400
7763.48	27	1.6	13	130	240	8	0.6	13	560	490
7837.42	43	2.9	12	440	220	25	2.0	10	520	300
7838.41	54	3.2	16	290	210	25	1.3	21	500	440
7839.38	42	3.3	11	330	190	14	1.3	10	320	300
8033.50	35	2.4	12	440	280	15	1.3	10	520	340
8035.48	46	3.5	12	350	270	17	1.3	12	430	320
8036.48	26	2.0	12	310	290	13	0.9	11	560	330
8037.48	19	1.4	13	140	200	8	0.5	16	480	320
	HeII λ 4686					HeIλ 4922				
6583.50	24	1.4	15	−20	−20	6	0.5	11	120	140
6584.45	14	0.7	19	−110	0	2	0.2	11	140	−30
6585.43	16	0.7	21	−180	−120	2	0.2	12	50	−40
6587.48	21	0.9	22	−140	−230	2	0.2	11	30	−90
6615.40	28	1.5	16	160	110	6	0.5	13	0	0
6616.51	40	1.8	20	110	20	8	0.5	15	190	200
6617.51	38	1.8	19	160	−60	9	0.5	21	−80	0
6620.51	32	1.7	16	90	110	7	0.4	10	−90	240
6621.46	28	1.3	23	270	350	7	0.5	14	260	400
6624.51	25	1.9	22	200	120	6	0.4	16	220	20
6953.41	15	0.8		−850	−650	4	0.3	10	480	190
7067.17	27	1.3	19	10	140	4	0.3	10	320	150
7068.20	20	0.8	25	40	270	2	0.2	11	350	240
7407.38	24	1.5	10	30	190	7	0.5	21	−440	−130
7408.32	17	0.8	21	50	−60	4	0.3	13	270	270
7410.38	38	1.2	28	50	−70	3	0.3	8	40	−160
7758.46	20	0.7	37	220	200	5	0.3	12	520	470
7759.54	24	0.8	33	250	−280	5	0.2	21	1030	380

JD 2440000+	W_λ (Å)	R_c	FWHM (Å)	V_c (km/s)	V_p (km/s)	W_λ (Å)	R_c	FWHM (Å)	V_c (km/s)	V_p (km/s)
7761.50	17	0.7	34	−10	590	5	0.4	14	330	370
7763.48	16	0.6	35	−10	570	3	0.2	14	440	410
7837.42	34	1.5	20	190	−30	3	0.3	13	220	290
7838.41	31	1.9	13	−70	10	3	0.2	17	280	150
7839.38	32	1.5	20	60	140					
7841.40	21	1.8	10	−270	−480					
8033.50	28	1.5	15	260	270	4	0.4	10	450	350
8035.48	32	2.0	14	210	220	5	0.5	11	320	280
8036.48	22	1.0	19	60	180	4	0.3	15	390	330
8037.48	17	0.8	16	−70	50	3	0.8	14	240	130
	HeI λ 5015									
6583.50	13	0.8	16	280	210					
6584.45	5	0.4	15	380	430					
6615.48	4	0.4	10	−70	−60					
6616.51	6	0.7	15	170	100					
6617.51	4	0.3	18	−90	160					
6620.51	10	0.5	17	−50	430					
6621.46	7	0.4	19	120	90					
6624.51	5	0.4	11	140	80					
7067.17	5	0.4	13	320	340					
7068.20	4	0.2	14	280	300					
7407.38	9	0.7	10	170	250					
7408.32	5	0.5	11	260	230					
7410.38	4	0.3	13	60	30					
7757.46	5	0.3	10	400	580					
7758.46	6	0.4	15	390	380					
7759.54	6	0.2	14	560	700					
7761.50	6	0.5	10	270	360					
7763.48	3	0.2	10	360	220					
7837.42	3	0.3	13	530	450					
7838.41	4	0.4	8	390	280					
7839.38	4	0.3	11	330	460					
8036.48	4	0.3	16	270	140					

Table 3: *Multicolour observations*

N	JD 2440000+	U	B	V	R	I	Comm.
II	6613.346	$16^m.58$	$15^m.98$	$13^m.81$	$11^m.60$	$10^m.34$	
	6620.329	17.07	16.16	13.97	11.68	10.41	
	6622.330	17.72	16.78	14.54	11.91	10.78	
	6625.309	17.07	16.23	14.08	11.73	10.52	
	6939.418	16.82	16.09	13.91	11.74	10.40	
	6940.378	16.63	15.71	13.57	11.38	10.09	
	6941.392	16.35	15.58	13.40	11.05	9.66	
	6944.376	17.08	16.22	13.99	11.78	10.36	
	6947.377	16.82	16.15	14.00	11.70	10.34	
	6951.379	16.89	15.97	13.79	11.54	10.22	

N	JD 2440000+	U	B	V	R	I	Comm.
IV	7403.216	16.84	16.06	13.88	11.63	10.41	
	7404.208	16.72	15.84	13.69	11.39	10.18	
	7405.206	16.41	15.61	13.45	11.08	9.96	
	7407.210	17.54	16.63	14.37	11.85	10.59	
	7408.209	17.42	16.54	14.31	11.97	10.65	
	7409.215	17.27	16.21	13.98	11.76	10.46	
	7410.185	17.04	16.11	13.95	11.79	10.44	
V	7756.230	–	–	14.15	11.88	–	ir
	7757.270	–	–	14.03	11.76	–	ir
	7757.297	–	–	13.96	11.77	–	m
	7758.210	17.30	16.25	14.06	11.87	10.56	
	7758.250	–	16.56	14.28	12.01	–	ir
	7758.276	–	–	14.12	11.96	–	m
	7759.220	17.22	16.37	14.16	11.95	10.65	
	7759.236	–	16.45	14.17	11.89	–	ir
	7759.354	–	–	14.22	11.93	–	m
	7760.220	17.30	16.59	14.34	11.88	10.61	
	7760.233	–	16.59	14.33	11.87	–	ir
	7761.220	17.64	16.58	14.37	12.07	10.84	
	7761.231	–	16.61	14.39	12.04	–	ir
	7761.310	–	–	14.51	12.16	–	m
	7762.169	17.26	16.37	14.15	11.88	10.62	
	7762.235	–	16.33	14.16	11.85	–	ir
	7763.310	–	–	13.92	11.79	–	m
	7767.229	–	16.04	13.91	11.65	–	ir
	7768.229	–	16.17	14.01	11.54	–	ir
VI	7836.187	–	16.84	14.59	–	–	sh
	7837.189	–	16.86	14.59	–	–	sh
	7838.185	–	16.89	14.68	–	–	sh
VII	8033.450	–	16.19	13.93	–	–	gr
	8034.464	–	16.84	14.48	–	–	gr
	8035.450	–	16.90	14.52	–	–	gr
	8035.450	–	–	14.52	12.17	–	ir
	8036.359	–	–	14.17	12.02	–	ir
	8036.456	–	16.40	14.28	–	–	gr
	8037.339	–	–	13.94	11.84	–	ir
	8037.481	–	16.00	13.92	–	–	gr
	8038.399	–	–	13.88	11.77	–	ir

Authors: V. Rakhimov (not marked), T. Manirov (m), S. Shugarov (sh), V. Goranskij (gr), T. Irsmambetova (ir).

The moments of spectral observations are marked by vertical bars. Different symbols correspond to different observers and are described in the figure captions. The differences in the fluxes on one night may be explained by both the fast variability of SS 433 and the differences in photometrical systems of the observers. The fast variability is known to be about $0^m.1$ in amplitude on time scales of 10–30 minutes, but it may reach $0^m.3$ (Goranskij et al., 1987; Irsmambetova, 1997). In the cases when we have more than 3 individual observations by one observer we show error bars in the figures, otherwise only average fluxes or colours are shown.

In Fig. 6 only the photometrical data of cycle I are plotted because we have no such data during cycle III. Fig. 7 presents the data obtained in cycles II and V and also the data obtained on JD 2446939 – 6951 (about the same precession phase as in cycles II and V). Fig. 8 shows the data of cycle IV, when we observed a strong burst of SS 433 lasting from $\varphi \approx 0.7$ to $\varphi \approx 0.0$. The flare had a neutral colour, as the colour indices behaviour did not change during these observations. In Fig. 9 we show the photometrical data obtained during cycles VI and VII. The high brightness difference of SS 433 in these observations is connected with the well–known precession variability (Gladyshev et al., 1987).

In all the eclipses we observe an increase in colour values B–V and, especially, V–R and V–I. This means eclipse of the hot body — the central part of the accretion disk. The notable changing of V–R and V–I is explained as the presence of additional red light, formed by free–free emission in the gas surrounding the binary system (Goranskij et al., 1997; Fabrika et al., 1997a; Dolan et al., 1997).

The examples of fast variability of SS 433 can be seen in Fig. 10, where we present individual observations obtained during cycle V at the Maidanak Observatory (filled circles) and at SAO (open circles). The variability amplitude grows towards blue wavelengths and amounts to $\pm 0^m.2$ in B–V. The high amplitude of B–V sporadical variability has been already discussed by Goranskij et al. (1997). More examples of the fast variability have been presented by Goranskij et al. (1987) among the data of cycle I, where we have the longest and homogeneous series of photometrical observations.

The fast variability of SS 433 can be clearly seen in Fig. 11a, where we present the continuous 2.2–hour long V–band light curve obtained with the three–beam, pulse–counting photometer on May 20, 1990 (cycle VII). The data were corrected for the contribution of the sky background and averaged with a 20 s window. The vertical axis is the relative magnitude V(SS 433)–V(BS). The total maximal amplitude of the SS 433 flux variability is about $0^m.25$, and a typical amplitude is about $0^m.1 \div 0^m.15$. The time–scales of the variability are from tens of seconds to about an hour. The Fourier power spectrum (Fig. 11b) has been calculated using Deeming's method (Loumos, Deeming, 1978). There are a number of peaks observed in the spectrum, in particular in Fig. 11b are presented the peaks (in units of 10^{-3} Hz): 0.13, 0.30, 0.62, 0.81, 1.74 (570 s), 3.48 (287 s), 4.90 (204 s). Some of the frequencies are obviously multiple. Because the data are strongly homogeneous, one may suggest that there is a real periodical (or quasi–periodical) signal in the flux variability of SS 433. The real period may exist among the short periods found in the data, probably 570 s. This particular period is presented in all the observing series. Two other short periods, 290 s and 200 s, seem to be multiple harmonics of the main 570 s period. We can conclude that these observations have shown that the SS 433 flux variability is probably periodical or quasi–periodical on a time scale of about a few minutes, and continuation of such observations is of great importance.

4. Results and discussion

The photometrical data have been used for the spectrum calibrations. In the cases when we had no photometrical data obtained on the same night as the spectra, we used the orbital and precession phase–averaged light curves and colour curves of SS 433 (Panferov et al., 1997). The procedure of spectrum calibration is standard (see for details the paper quoted). In Figs. 12–16 we present fragments of all the spectra in the region $\lambda\lambda$ 4600–5050. The spectra have been corrected for interstellar absorption, assuming for SS 433 $A_V = 7^m.85$ (Cherepashchuk et al., 1982; Dolan et al., 1997). The spectra presented are in units of 10^{-11} erg/cm^2 s Å and they are shifted along the vertical axis for a better presentation (see the figure captions for details). There are stationary lines in the spectral region in Figs. 12 – 16: C III, N III $\lambda_{\rm eff}$ 4644, He II λ 4686, Hβ and He I λ 4922. In the spectra of eclipses I and III (Fig. 12) one can see the moving relativistic line Hδ^+ whose position is marked by vertical bars. The position of another moving line Hϵ^+ is also marked there. The precession and orbital phases of cycles I and II are about the same, nevertheless, their spectra are different in the blue wing of Hβ. During eclipse I we observe the blue absorption component, but in eclipse III we observe additional emission in the blue wing. In cycles II and V in Fig. 13a, b the situation in this region is more complicated, as Hβ^- and Hγ^+ lines pass through the region. The He II and Hβ line profiles are often distorted by the moving emissions or by their traces. In cycle IV (Fig. 14) the positions of the moving lines are similar to those of cycles I and III. During eclipse VI (Fig. 15) the strong line Hβ^- distorts the Hβ line profile. The only moving line Hδ^+ moves across this region during cycle VII

Table 4: *V-band observations*

N	JD 2440000+	V	Comm.	N	JD 2440000+	V	Comm.
IV	7403.247	$14^m.19$	pe	V	7756.323	$14^m.00$	ph
	7404.250	13.91	pe		7758.353	14.12	ph
	7405.303	13.69	pe + ph		7759.369	14.28	ph
	7406.343	14.11	pe		7760.364	14.27	ph
	7407.353	14.44	pe + ph		7761.356	14.45	ph
	7409.357	14.11	ph		7762.338	14.26	ph
	7410.335	14.05	ph	VII	8031.485	13.92	m
	7411.243	14.23	ph		8033.494	13.96	m
					8035.471	14.75:	m
					8036.476	14.25	m

Observations by V. Goranskij and photoelectric observations by T. Manirov (m).

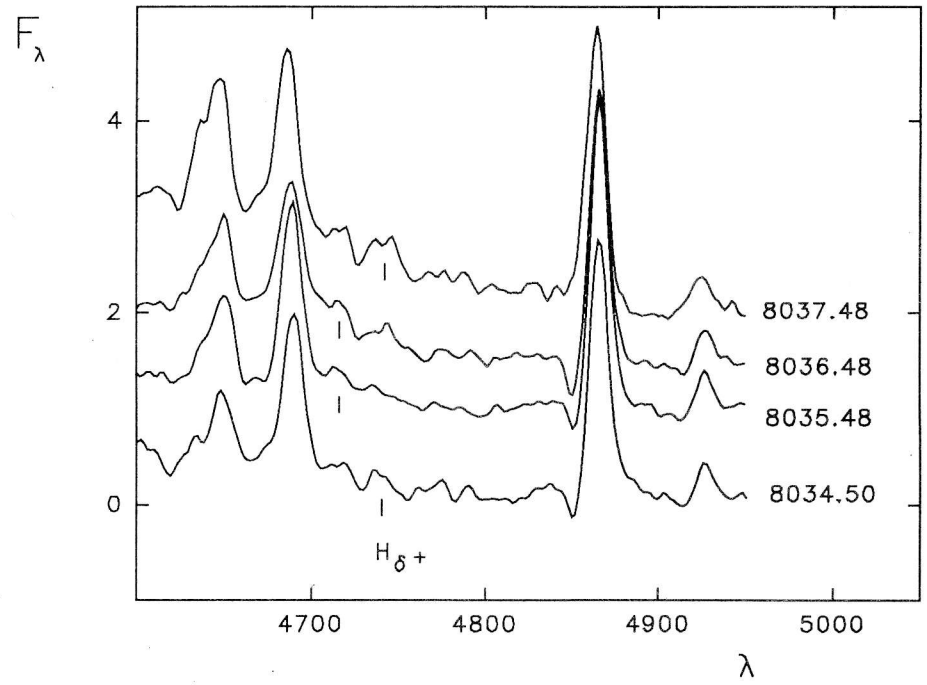

Figure 16: *Fragments of the spectra of SS 433 obtained in cycle VII. The spectrum for JD 2448034.50 was shifted along the vertical axis on −1. The units are the same as in Fig. 12.*

(Fig. 16).

It has been found (Goranskij et al., 1997; Fabrika et al., 1997 a) from the data of cycles I and III, that the He II λ 4686 line is eclipsed twice at the orbital phases $\varphi = 0.0$ and 0.1. It becomes narrow (and practically Gaussian) in the middle of the photometrical minimum Min I. Later, on increasing branch at $\varphi \approx 0.1$ the line becomes broader, the broad blue and red line components appear, but at the same moment the narrow intensive component in turn enters the eclipse. So, it has been found that the line consists of at least two components: a broad and double-peaked one, which is totally eclipsed at $\varphi = 0.0$ (formed in the middle of the accretion disk or in the "He II cocoons" around the relativistic jet bases) and a narrow, more intensive component, which is partially eclipsed at $\varphi \approx 0.1$ (formed in a gas stream, directed to the disk). This behaviour of the He II line is very well seen in Fig. 12 b and Fig. 14 in the spectra of cycles I and IV studied earlier. Such a scenario is repeated in the spectra of cycle VII in Fig. 16, where the He II line profile looks narrow and intensive in the middle of the eclipse (JD 2448035, $\varphi = 0.019$), but broader and less intensive on the next and previous nights.

In cycle VI (Fig. 15) this line again becomes narrower, when the accretion disk enters its eclipse, but it becomes broader on the next night, when the disk is still in the middle of the eclipse. In cycles II and V (Fig. 13) the He II line profile is distorted too strongly by the moving line $H\beta^-$ so as to draw any conclusions on the line profile variability. Goranskij et al. (1997), Fabrika et al. (1997 a) have also discussed eclipses of the $H\beta$ line. The light curve of the $H\beta$ flux eclipse has been found to be broader than that of He II with the centre at the orbital phases $\varphi = 0.1 \div 0.2$. The $H\beta$ line eclipse is partial.

In Fig. 17 the He II line fluxes and widths are plotted. The fluxes are in units of 10^{-10} erg/cm^2 s. Each cycle plotted is marked by the different symbols. If this line was distorted by moving lines, such data were omitted in the figure. Nevertheless because of the different states of activity and different precession phases of the orbital cycles, the individual curves in the figure are notably different. For example, during cycle V the He II line (squares in the figure) was about twice as broad as usual, but its total flux did not notably change.

In order to see general trends and the line behaviour through the primary minima, we present the data averaged in the orbital phase bins (big open circles in Fig. 17). It is obvious that the averaged data confirm the eclipse to be present at the orbital phase $\varphi = 0.0 \div 0.1$. This is not symmetrical, a portion of the total line flux is already eclipsed at $\varphi = 0$, but the main minimum is reached at $\varphi \approx 0.1$. The line width shows a minimum at $\varphi \approx 0.0$ (Fig. 17 b, the data of cycle V were not taken into account), when the broad line component is eclipsed, and it shows a maximum at $\varphi \approx 0.1$, where the narrow line component of He II is partially eclipsed. So the data confirm the conclusion which have been drawn before (Goranskij et al., 1997; Fabrika et al., 1997 a) on the basis of the study of eclipses I and IV alone.

In Fig. 18 the $H\beta$ line fluxes and widths are plotted. The units, designations and method are the same as in the previous figure. The line flux is obviously decreased at $\varphi = 0.1 \div 0.2$. The $H\beta$ line eclipse looks broader and is delayed relative to the eclipse of the He II line. The main portion of the He II line flux and probab y all the $H\beta$ line flux are formed in the gas stream. Fabrika et al. (1997 a) have concluded from the line light curves that the stream is directed to the accretion disk because the stream head is closer to the disk and hotter than the main stream body. The data confirm this conclusion. The average $H\beta$ width, in spite of the strong variability of individual points (Fig. 18 b), does not show notable regular variability in the orbital phase interval $\varphi = 0.9 \div 1.2$. Probably the line is a little narrower at the phases $\varphi = 0.0 \div 0.1$.

Absorption P Cyg–type line components appear

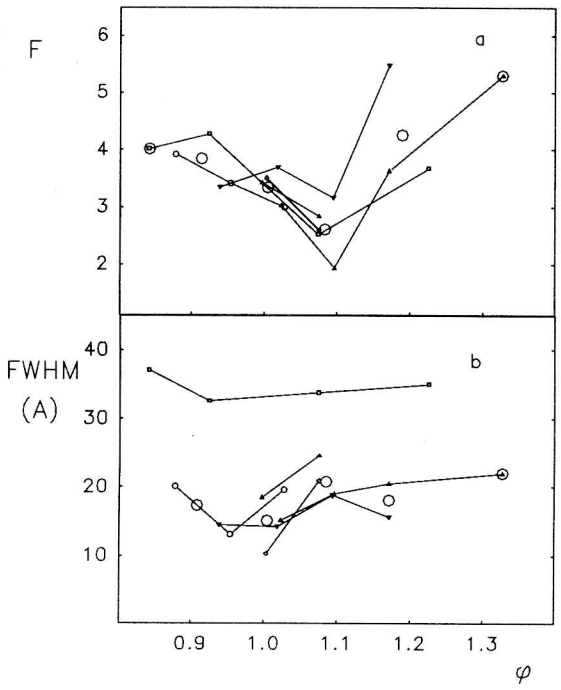

Figure 17: *The He II λ 4686 line fluxes (a) and widths (b) versus the orbital phase. The fluxes are in units* 10^{-10} erg/cm^2 s. *Cycles I and III — triangles, IV — diamonds, V — squares, VI — little circles, VII — turn over triangles. The data averaged in the orbital phase bins are shown by big open circles. In* $\varphi \approx 0.0$ *the broad He II component is eclipsed, and in* $\varphi \approx 0.1$ *the narrow component is eclipsed.*

in the line profiles of H I, He I and Fe II (Crampton, Hutchings, 1981; Fabrika et al., 1997 b) in the precession phase interval $\psi \approx 0.3 \div 0.9$, which is around the accretion disk "edge–on" orientation. Fabrika et al. (1997 b) have found that these lines are formed in the accretion disk wind. The wind velocity depends on the disk polar angle. This results in variations of radial velocities of the absorption lines with precession phase: from 100 – 150 km/s in the disk plane to about 1200 km/s at a polar angle of $\approx 60°$. The moment of the absorption line appearance in the SS 433 spectrum is delayed by $\Delta\psi = 0.1 \div 0.15$ relative to the centre of symmetry of the true "edge–on" position, $\psi = 0.5$. Fabrika et al. (1997 b) explained this time delay as a time, which is needed for absorption gas to be accumulated on the line of sight for a notable absorption line to appear.

The appearance of absorption lines in the SS 433 spectrum is connected not only with the disk edge–on orientation. One can conclude from Figs. 12 – 16, that the blue–shifted absorption line components of the strongest line $H\beta$ appear (or their intensity is enhanced) at the orbital phases near the primary min-

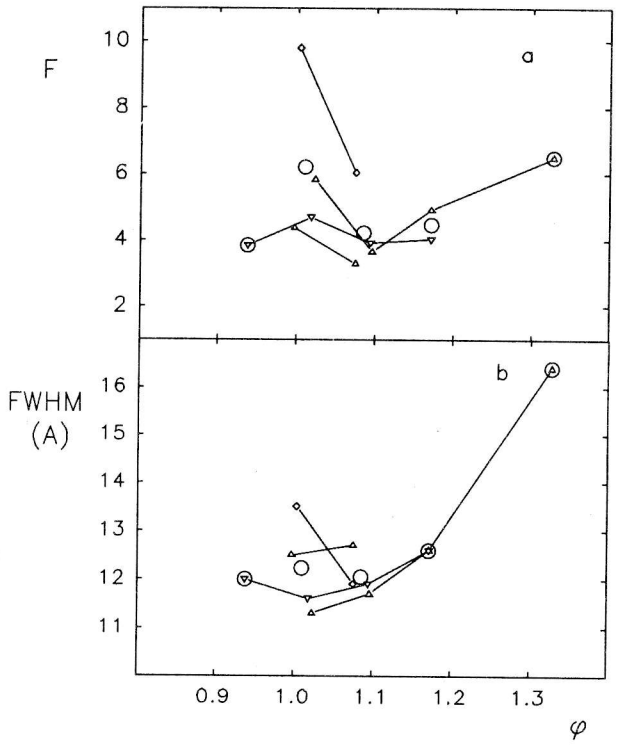

Figure 18: *The Hβ line fluxes (a) and widths (b) versus the orbital phase. In other respects the same as in Fig. 17. The Hβ line eclipse is delayed relatively that of the He II line.*

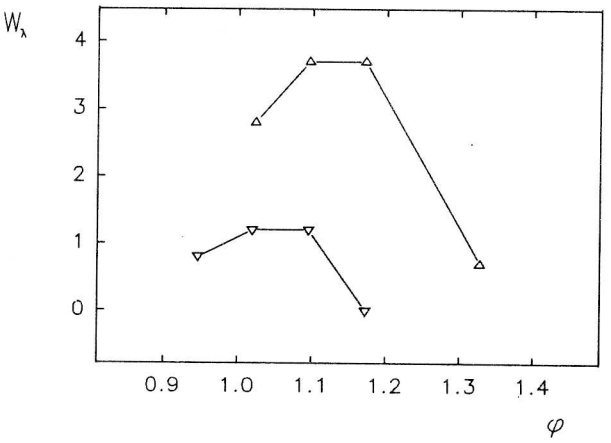

Figure 19: *The Hβ absorption line equivalent widths in Å versus the orbital phase. The precession phases of the observations are $\psi = 0.94$ (cycle I, triangles) and $\psi = 0.87$ (cycle VII, turn over triangles).*

imum. The obvious examples of this are in Fig. 12 b (cycle I, $\psi \approx 0.94$), in Fig. 15 (cycle VI, $\psi \approx 0.66$, but the Hβ line profile is distorted there by the moving Hβ$^-$ line) and in Fig. 16 (cycle VII, $\psi \approx 0.87$). In Fig. 12 a (cycle III, $\psi \approx 0.91$) and in Fig. 14 (the cycle IV, $\psi \approx 0.01$) we observe an emission hump in the blue wing of the line profile instead of the absorption component. The He I λ 4922 line profile, though it is more noisy registered, is similar to the Hβ profile in all the spectra. In Fig. 13 a (cycle II) and in Fig. 13 b (cycle V) the precession phase $\psi \approx 0.1 \div 0.2$, and no absorption components are observed, but at these phases the Hβ profile may be distorted by the Hγ$^+$ line.

We suggest that the absorption line intensity grows at the primary photometrical minima. To check this, we present in Fig. 19 the equivalent widths of the Hβ absorption line components versus orbital phase for cycles I and VII where the line was not distorted by moving lines. The equivalent widths were calculated from the level of the continuum, so they could be only considered as estimates of this value. The precession phases are close to 0, this means the high wind velocities on the line of sight at these moments (Fabrika et al., 1997 b). The absorption line strengths show a maximum, which is delayed relative to the Min I ($\varphi = 0$). The delay is probably connected with the precession phase (the wind velocity) and amounts to $\Delta\varphi \approx 0.05$ in cycle VII at $\psi = 0.87$ (the wind velocity $V_{ej} \approx -500$ km/s) and $\Delta\varphi \approx 0.15$ in cycle I at $\psi = 0.94$ ($V_{ej} \approx -1200$ km/s).

This transient increasing of the absorption line intensity may be a manifestation of a trail behind the optical star. The low–density and high–velocity wind (at these disk latitudes) interacts with the optical star. With such a perturbation of the wind its gas density may rise making possible formation of notable absorption lines. The phase delay $\Delta\varphi$ (the trail curvature) must depend on the wind velocity.

The main aim of the paper was the presentation of the observational data. We suppose to publish in the next paper an analysis of the He II and Hβ line profile variations through the accretion disk eclipses in the seven orbital cycles presented.

Acknowledgements. The authors are thankful to N.V. Borisov for assistance in spectral observations. This work has been supported by grant N 3-13 of the Programme "Astronomy".

References

Borisov G.V., 1992, Astron. Astrophys., **261**, 154

Cherepashchuk A.M., Aslanov A.A., Kornilov V.G., 1982, Astron. Zh., **59**, 1157

Crampton D., Hutchings J.B., 1981, Vistas in Astron., **25**, 31

Dolan J.F., Boyd P.T., Fabrika S., Tapia S., Bychkov V.D., Panferov A.A., Nelson M.J., Percival J.W., van Citters G.W., Taylor D.C., and Taylor M.J., 1997, Astron. Astrophys., in press

Drabek S.V., Kopylov I.M., Somov N.N., Somova T.A., 1986, Astrofiz. Issled. (Izv. SAO), **22**, 64

Gladyshev S.A., Goranskij V.P., Cherepashchuk A.M., 1987, Sov. Astron., **64**, 1037

Gladyshev S.A., Irsmambetova I.R., 1989, Prepr. of Sternberg Institute, **7**

Goranskij V.P., 1987, Astronomical Circ., **1153**

Goranskij V.P., Kopylov I.M., Rakhimov V.Yu., Borisov N.V., Bychkova L.V., Fabrika S.N., Chernova G.P., 1987, Soobshch. Spets. Astrofiz. Obs., **52**, 5

Goranskij V.P., Fabrika S.N., Rakhimov V.Yu., Panferov A.A., Belov A.N., Bychkova L.V., 1997, Astronomy Reports, in press

Fabrika S.N., Kopylov I.M., Shkhagosheva Z.U., 1990, Prepr. of the Special Astrophys. Obs., **61**

Fabrika S.N., Panferov A.A., Bychkova L.V., Rakhimov V.Yu., 1997 a, Bull. Spec. Astrophys. Obs., **43**, (this issue), 95

Fabrika S.N., Bychkova L.V., Panferov A.A., 1997 b, Bull. Spec. Astrophys. Obs., **43**, (this issue), 75

Irsmambetova T.R., 1997, Astronomy Letters, **23**, 341

Kayumov V.V., Kiselev N.N., Pushnin P.A., Rakhimov V.Yu., Siklitskij V.I., Tarasov K.V., Chernova G.P., Yakutovich V.N., 1989, Bull. of the Tadjik Institute of Astrophys., **78**, 10

Kopylov I.M., Kumaigorodskaya R.N., Somov N.N., Somova T.A., Fabrika S.N., 1987, Sov. Astron., **64**, 785

Kopylov I.M., Bychkova L.V., Fabrika S.N., Somova T.A., Kumaigorodskaya R.N., 1989, Sov. Astron. Lett., **15**, 474

Kopylov I.M., Kumaigorodskaya R.N., Somov N.N., Somova T.A., Fabrika S.N., 1986, Sov. Astron., **63**, 690

Kopylov I.M., Kumaigorodskaya R.N., Somova T.A., 1985, Sov. Astron., **62**, 323

Loumos G.L., Deeming T.J., 1978, Astrophys. Space Sci., **56**, 285

Neizvestny S.I., Pimonov A.A., 1978, Soobshch. Spets. Astrofiz. Obs., **23**, 39

Neizvestny S.I., Pustilnik S.A., Efremov V.G., 1980, Sov. Astron. Lett., **6**, 700

Margon B., Anderson S.F., 1989, Astrophys. J., **347**, 448

Panferov A.A., Fabrika S.N., Rakhimov V.Yu., 1997, Astronomy Reports, **74**, 392.